Development of a carbon quantum dot-based sensor for the detection of acetylcholinesterase and the organophosphate pesticide

Niloofar Mahmoudi, Fataneh Fatemi [*], Moones Rahmandoust [**], Fateme Mirzajani, Seyed Omid Ranaei Siadat

Protein Research Center, Shahid Beheshti University, Tehran, Iran

ARTICLE INFO

ABSTRACT

In this study, a proper and reliable fluorometric method is introduced for screening acetylcholinesterase (AChE) and its inhibitors, using carbon quantum dots (CQDs) as the signal reporter. Pure, S-doped, and P-doped CQDs, were synthesized and their recoverable fluorescence quenching properties were observed, when exposed to Hg^{2+}, Cu^{2+}, and Fe^{3+} quenching ions, respectively. The study on the recovery of their emission showed that after the introduction of another guest substance with a stronger affinity to the quenching ions, their fluorescence is restored. The Design Expert software was employed to compare the performance of the three CQDs, as fluorescent probes, based on their quenching efficiency and the percentage of their emission recovery in the presence of AChE and acetylthiocholine (ATCh). Based on the statistical analysis, among the studied CQDs, S-doped CQD was the most suitable candidate for sensor designing. The detection mechanism for the proposed S-doped CQD-based sensor is as follows: The strong binding of Cu^{2+} ions to carboxyl groups of S-doped CQD quenches the fluorescence signal. Then, hydrolysis of ATCh into thiocholine (TCh) in the presence of AChE causes fluorescence recovery, due to the stronger affinity of Cu^{2+} to the TCh, rather than the CQD. Finally, in the presence of malathion and chlorpyrifos inhibitors, AChE loses its ability to hydrolyze ATCh to TCh, so the fluorescence emission remains quenched. Based on the proposed detection technique, the designed sensor showed detection limits of 1.70 ppb and 1.50 ppb for malathion and chlorpyrifos, respectively.

1. Introduction

Acetylcholinesterase (AChE) is a vital enzyme in the central nervous system that catalyzes the hydrolysis reaction of the neurotransmitter acetylcholine (ACh) to choline and acetic acid [1], thereby helping to maintain ACh levels [2,3]. Moreover, AChE is present in muscle and peripheral tissues, motor, sensory, cholinergic, and non-cholinergic fibers [4–6]. Its main biological role is to terminate the transmission of neural messages at cholinergic synapses by ACh hydrolysis [7,8]. Inhibition of AChE leads to the accumulation of ACh, which leads to the permanent saturation of its receptors and the creation of a cholinergic crisis throughout the central nervous

system. The overstimulation of the cholinergic system can cause many symptoms such as paralysis, seizures, and respiratory failure, which may finally lead to death [9]. Organophosphorus pesticides (OPs) are potent irreversible AChE inhibitors that covalently bind to serine residues at the AChE's active site, thereby inhibiting AChE's activity [10–12]. OP pesticides are classified as extremely dangerous compounds, with a broad spectrum of toxicity types, by the World Health Organization (WHO). Among the various OPs, malathion is a common insecticide that is used due to its low toxicity [13], rapid degradation, and excellent efficacy [14]. It is widely used to increase the storage time of grains by controlling or eradicating diseases caused by arthropods [15], foreign animal parasites, and domestic insects [15,16]. The mechanism of malathion toxicity is through AChE inhibition [17,18]. To eliminate pests, about 1% of the introduced toxic malathion is used [19] and the excess remains there [20], as a pollutant on the soil and water resources, making serious damage to the human nervous, respiratory and cardiovascular systems [14]. It may also develop some other symptoms such as tingling sensation [21], headache [22], dizziness [23], worsening of asthma [24], paralysis [25], or even death [26]. Moreover, the formation of free radicals is one of the main toxicity phenomena observed from OPs [27]. Chlorpyrifos, as another OP insecticide used against agricultural pests, attacks the hydroxyl serine group at the active site of AChE, and inhibits it irreversibly [28,29]. This reaction leads to the accumulation of the neurotransmitter ACh and ultimately to neurotoxicity [30]. These pesticides are absorbed rapidly through the respiratory, gastrointestinal, ocular, and dermal pathways, with absorption after inhalation as the fastest way. Their absorption through the skin is, however, slower, leading to severe poisoning over long-term exposure [31]. Due to the mentioned issues, including the high carcinogenic and genetic toxicity potential, control of the excess OPs on plants, crops, soil, and water is essential and accurate monitoring of their concentrations in the environment and biological sample has become of utmost importance [20].

Hence, various investigations employing a variety of techniques, including colorimetric, electrochemical, interferometric, chemiluminometric, and fluorometric methods have been performed to measure the activity of AChE and its inhibitors, [32–36]. However, the developed techniques are generally lack enough sensitivity. For example, the Elman reagent that used currently in the colorimetric measurement leading to false positive results [33]. In order to increase the sensitivity and decrease the limit of detection, dye molecules were employed in chemiluminometric or fluorometric approaches [37–41]. However, dyes have their own inherent disadvantages, including rapid bleaching, insufficient diffusion intensity, and instability. In recent years, several new fluorescent materials, such as noble metal nanoparticles [42–46], mineral quantum dots [47,48], and fluorescent conjugated polymers or proteins [49–51] have been used to measure the activity of AChE inhibitors. Although these fluorescent materials have properties such as high fluorescence quantum efficiency, strong absorption, and emissions, as well as good performance for measuring AChE activity, there is still high demand for simple, low-cost, unlabeled, and sensitive assays to detect AChE and its inhibitors in biological samples.

Carbon quantum dots (CQDs), as a novel type of carbon-based nanomaterials, have also attracted significant attention, due to their distinctive optical properties and excellent performance in photovoltaic, photocatalytic, and bioimaging applications [52–54]. CQDs have exhibited promising properties such as stable light emission, high quantum efficiency, good light stability, easy modulation, low toxicity, and excellent biocompatibility [55], which makes them excellent fluorophores in fabricating novel fluorescent chemo/-biosensors that are, suitable for *in vitro* and *in vivo* applications [56–58]. Recent studies have shown that CQDs can be successfully used to create fluorescent assays to evaluate the activity of several enzymes such as protein kinase [59], hyaluronidase [60], alkaline phosphatase [53,61], and AChE [37]. However, the developed techniques are generally time-consuming and showed a long processing time. Based on the current state of knowledge, this study aimed to develop a convenient and highly sensitive fluorescent method for screening AChE and its organophosphate inhibitors of malathion and chlorpyrifos, using CQDs.

2. Experimental

2.1. Materials and chemicals

Citric acid monohydrate, sodium hydroxide, phosphoric acid, copper sulfate ($CuSo_4$), iron chloride ($FeCl_3$), mercury chloride ($HgCl_2$), trisodium citrate dihydrate, sodium thiosulfate, acetylcholinesterase and acetylthiocholine, bovine serum albumin (BSA), alkaline phosphatase (ALP), DNA, and sodium chloride (NaCl) were purchased from Merck, Germany and Sigma-Aldrich, Netherlands, and used without further purification.

2.2. Synthesis of CQDs

2.2.1. Synthesis of pure CQD

An aliquot amount of 0.2 g citric acid monohydrate was dissolved in 20 mL of distilled water and then, the solution was transferred to a hydrothermal reactor, being heated in an oven for 5 h at 180 °C. After cooling down to room temperature, 2.0 M sodium hydroxide was used to neutralize the solution. The synthesized pure CQDs were kept at 4 °C before freeze-drying.

2.2.2. Synthesis of S-doped CQD

1.2 g of trisodium citrate dihydrate and 2.3 g of sodium thiosulfate were dissolved in 50 mL distilled water and the solution was transferred to a hydrothermal reactor for synthesis of S-doped CQDS at 200 °C for 6 h. At the end of the chemical reaction, the hydrothermal reactor was left to cool down to 25 °C [62]. The synthesized S-doped CQDs were kept at 4 °C before freeze-drying.

2.2.3. Synthesis of P-doped CQD

For P-doped CQD synthesis, 1.5 g of sucrose was dissolved in 30 mL of distilled water and 2 mL of 1.0 M phosphoric acid, under

stirring to obtain a clear solution. Afterward, the solution was transferred to a hydrothermal reactor and heated at 200 °C for 5 h. Thereafter it was left to cool down to room temperature and then centrifuged at 10 k rpm for 30 min to separate large insoluble particles. Finally, pH adjustment was done with 1.0 M sodium hydroxide [63]. The synthesized P-doped CQDs were kept at 4 °C before freeze-drying.

2.3. Characterization of the CQDs

The particle size and its distribution were determined using transmission electron microscopy (TEM, JEOL 2200FS, Tokyo, Japan) and dynamic light scattering (DLS, Nanoparticle Analyzer HORIBA SZ-100, Kyoto, Japan). The zeta potential was also measured in three replications, using the later instrument. The photoluminescence (PL) and x-ray photoelectron spectroscopy (XPS) measurements were performed using spectrophotometer (PerkinElmer LS45, Massachusetts, USA) and (XPS, PHI 5000 Versaprobe, Physical Electronics, USA), respectively. An x-ray powder diffraction (XRD, Rigaku Ultima IV Tokyo, Japan) was used to study of crystal structures and crystalline interlayer distances, and the functional groups of each CQD were obtained using Thermo Nicolet, NEXUS 470 (Illinois, USA) Fourier Transform Infrared (FTIR) spectroscopy.

2.4. Experimental design

Design Expert software (version 7.0.0) was used over the central composite design (CCD) algorithm to compare the intensity variation of CQD's emission in terms of maximum emission and quenching rates, under AChE and quenching ion treatments. For that, two quantitative factors; namely, the interaction time duration (A, in min) and the volume ratio of CQD to AChE enzyme (CQD/En ratio) (B, in %), and one qualitative factor, i.e. the CQD type (C), were considered. The influence of the interactions on CQD performance was monitored using the enzyme-linked immunosorbent assay (ELISA, BioTek Cytation 5, USA) as a response (Table 1).

A total of 33 experiments, containing three center points and eight non-center points (overall 11 experiments) for each CQD was performed as presented in Table 2. The concentration of stock solution for AChE and ATCh in each excrement was 100 U/µL and 0.5 mM, respectively. The pure, S-doped, and P-doped CQD solutions had initial concentrations of 17.5 mg/mL, 11 mg/mL, and 2.5 mg/mL, respectively. The final concentrations were adjusted according to Table 2, using phosphate-buffered saline (PBS) for pure, S-doped, and P-doped CQDs and excited at 360 nm wavelength. Thereafter, the CQD's maximum emissions wavelengths were monitored to be at 446, 436, and 417 nm in the cases of pure, S-doped, and P-doped, respectively. In the next step, the quenching percentage was obtained for each CQD, using aliquot amounts of identified quenching ions. Finally, 50 µL of AChE and 1.5 µL of ATCh were added and after the appropriate designed time, the emission intensity variation was monitored in each CQD. The effect of these treatment steps was studied based on two responses of emission and quenching percentages. Since both responses had equal importance, the desirability function (D_f) was defined and calculated according to (Eq. (1)). In this way, the values of both responses are evaluated equally and simultaneously. In this equation, Q is the percentage of quenching, and I is the percentage of CQD emission intensity.

$$D_f\% = \sum (0.5 \times Q\%) + (0.5 \times I\%) \tag{1}$$

2.5. Detection of AChE and OP pesticides

The results of fluorescence emission and quenching of CQDs were recorded. According to the results, the experiment was selected to be continued using the S-doped CQD as the fluorescent probe for identifying malathion and chlorpyrifos OPs. According to the regulations of the WHO, the maximum acceptable and permissible amount of malathion and chlorpyrifos on the environmental resources are 50 ppb and 10 ppb, respectively. However, much lower concentrations of 0.000, 0.005, 0.030, 0.050, 0.090, 0.150, 0.220, 0.300 ppb were selected for malathion and 0.000, 0.002, 0.020, 0.070, 0.100, 0.150, 0.200, 0.250 ppb for chlorpyrifos. The experiments were performed in three replications for both OPs, giving the sensing system 30 min for the interactions of the components. Limit of detection (LOD) is one of the results that obtained from the calibration curves using following equation:

$$\text{LOD} = \frac{3sb}{m} \tag{2}$$

where Sb is the standard deviation for blank and m is the slope of calibration curve.

Table 1
Factors together with theis notations and levels for the central composite design.

Factor names		-α*	−1	0	+1	+α[a]
A	Interaction time (min)	0.3	3	9.5	16	18.7
B	**CQD/En ratio (%)**	1.5	4	10	16	18.5
C	**CQD Type**	Pure		S-doped	P-doped	

[a] α = 0.2.

Table 2
Designed experiments to study the influence of CQD on the detection of AChE and its inhibitors.

Std*	Run order	Time (min)	CQD/En ratio (%)	CQD type	D_f %**
14	1	3	16	S-doped	34.01884
8	2	9.5	18.5	Pure	29.73972
15	3	16	16	S-doped	29.04908
24	4	16	4	P-doped	27.19716
10	5	9.5	10	Pure	32.89456
27	6	0.3	10	P-doped	31.78781
6	7	18.7	10	Pure	27.96525
29	8	9.5	1.5	P-doped	29.45529
25	9	3	16	P-doped	31.10656
12	10	3	4	S-doped	33.52306
19	11	9.5	18.5	S-doped	31.17059
1	12	3	4	Pure	37.05767
18	13	9.5	1.5	S-doped	32.66461
26	14	16	16	P-doped	26.05196
9	15	9.5	10	Pure	29.05567
28	16	18.7	10	P-doped	25.49794
3	17	3	16	Pure	30.24026
17	18	18.7	10	S-doped	31.26231
22	19	9.5	10	S-doped	29.20168
20	20	9.5	10	S-doped	32.02089
33	21	9.5	10	P-doped	27.97358
30	22	9.5	18.5	P-doped	25.51604
16	23	0.3	10	S-doped	33.58546
31	24	9.5	10	P-doped	32.56716
21	25	9.5	10	S-doped	31.25895
5	26	0.3	10	Pure	33.61139
7	27	9.5	1.5	Pure	35.37244
23	28	3	4	P-doped	28.97916
4	29	16	16	Pure	29.18125
32	30	9.5	10	P-doped	30.17559
2	31	16	4	Pure	29.4359
13	32	16	4	S-doped	31.98053
11	33	9.5	10	Pure	30.63094

Std: Standard deviation **D_f: Desirability function.

3. Results and discussions

3.1. Characterization of CQDs

3.1.1. Characterization of Pure CQDs

The average particle size of pure CQDs was obtained using TEM and the zeta potential using DLS instrumentations. The results show a relatively uniform distribution of particles of 4.9 ± 2.7 nm with a surface charge of -19.1 ± 2.3 mV (Fig. 1a and b). Based on the XPS and FTIR results, the high negative charge is related to the negatively charged C–O groups. FTIR spectrum reveals the stretching vibrations of C–O (1310 and 1250 cm^{-1}), aromatic C=C bond's stretching, and bending frequencies (1560 and 842 cm^{-1}) and C–H bending (1377 cm^{-1}) (Fig. 1c). The XPS study data on the pure CQD composition shows a major peak with 50.9% of atomic percentage at around 283.30 which corresponds to C1s (C=C aromatic) and another one at 530.69 eV, showing 49.1% of O1s (C–O) (Fig. 1d). XRD results (Fig. 1e) show that the crystal plates (002) are detectable at angles of 2θ between 20 and 26° with 3.14 nm d-spacing between the crystal plates, as observed in TEM image. The pure CQDs have a maximum PL absorption at 365 nm and a visible emission at 446 nm (Fig. 1f).

3.1.2. Characterization of S-doped CQDs

According to the TEM, DLS, and Zeta potential results, the average particle size of S-doped CQDs is 1.30 ± 0.6 nm (Fig. 2a and b), and the surface charge is -2.6 ± 1.1 mV. In the case of S-doped CQDs, a rather inhomogeneous distribution of size is observed. FTIR spectra were used to identify the functional groups of the S-doped CQD. As shown in Fig. 2c, the O–S bond of organic sulfate is significant between 1370 and 1420 cm^{-1} and C–O bending 1150-1085 cm^{-1}. The XPS spectrum (Fig. 2d) shows a relatively 19.3% of sulfur, which is relatively high. The C1s spectrum shows that the C=C sp2 bonds, covering 79.4% of the spectrum, are the most dominant bindings, observed at 283.55 eV. The S bonds are revealed in the high-resolution S2p XPS results, as the S=O bond at the binding energy of 168.89 eV and the C–S–C bond at 162.68 eV. The XRD (Fig. 2e) shows the (002) crystalline plate. The (102) graphitic carbon crystalline phases are remarkable between 40 and 50°, and (004) is placed between 50 and 55°. The distance between the crystal plates is equal to 3.18 nm in S-doped CQDs. The optical properties of water-dispersed S-doped CQDs are shown in Fig. 2f. Maximum absorption is observed at 356 nm and two PL emission wavelengths are recorded at 436 and 732 nm.
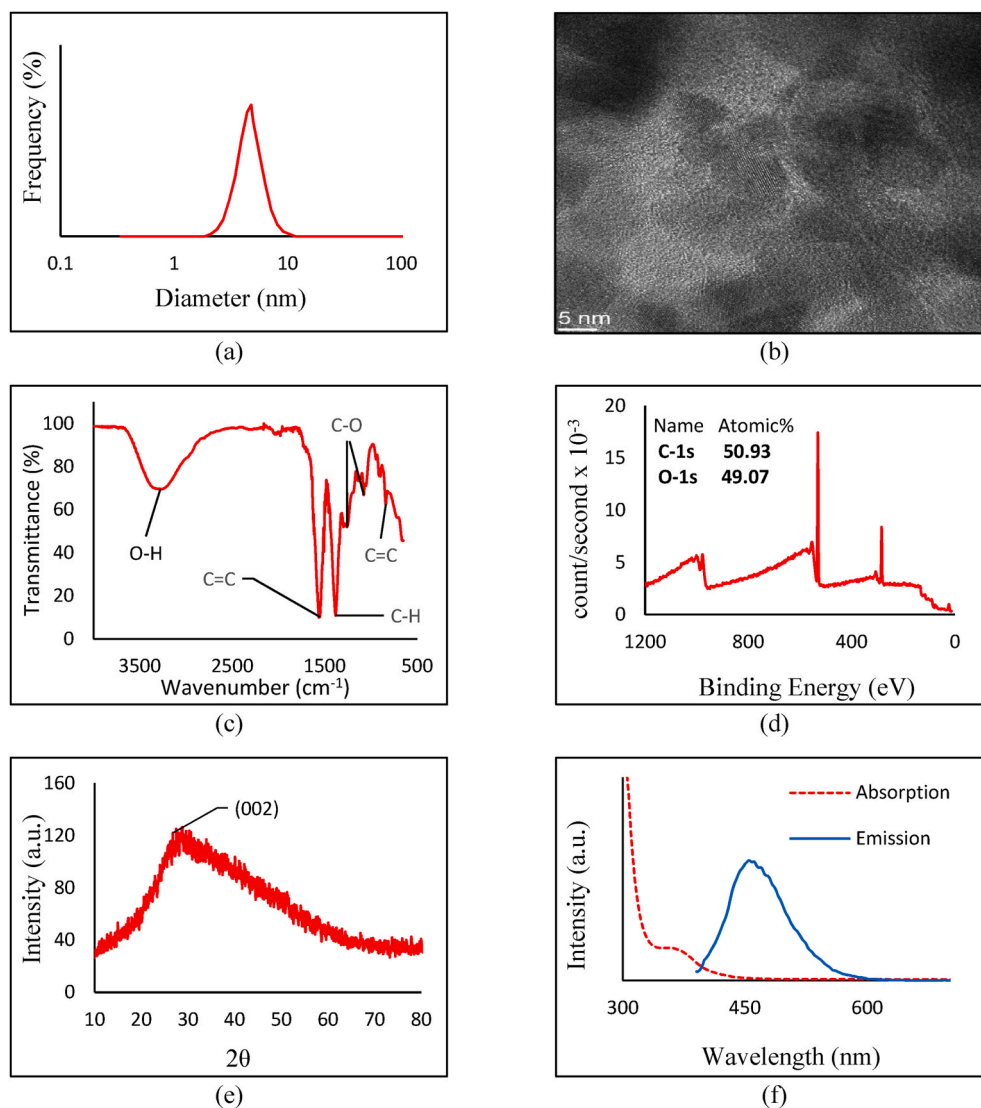
Fig. 1. Characterization of Pure CQD: (a) DLS, (b) TEM, (c) FTIR, (d) XPS, (e) XRD, and (f) PL absorption/emission diagrams.

3.1.3. Characterization of P-doped CQDs

As shown in Fig. 3a and b, a uniform distribution of P-doped CQD particles with an average diameter of 1.15 ± 0.05 nm is observed, with a surface charge of -19.3 ± 2.0 mV. The FTIR spectrum (Fig. 3c), shows an apparent absorption peak at about 1146 cm^{-1}, attributed to P═O vibration, and at 1581 cm^{-1} to P–C vibration. Simultaneously, the C═C tensile vibration absorption band appeared at 2119 cm^{-1}. The XPS analysis of P-doped CQDs (Fig. 3d), confirms the existence of 46.7% of carbon and 40.9% of oxygen as the most dominant atoms, accompanied by a high content of phosphorous doping (12.3%) in the structure of the CQD. As also admitted by notable vibrations in the FTIR results, the P heteroatom doping (P–O bond) is observed at 284.74 eV in O1s, and at 132.8 eV in P2p diagrams. The C═O bond on the other hand is observed in the C1s, at 286.70 eV, and in the O1s at 529.89 eV binding energies. The C–C bond can be seen as sp2 configuration at 283.48 eV in the C1s diagram. The X-ray powder diffraction (Fig. 3e) shows that in the range between 20 and 30°, the (002) crystalline plate can be seen and the (004) is placed between 50 and 55°. Furthermore, the distance between the crystalline plates is about 2.80 nm in P-doped CQD. A UV–vis absorption at 360 nm and two strong fluorescence emission peaks at 417 and 727 nm are observed, indicating that P-doped CQDs are capable of emitting visible light when excited by UV electromagnetic waves (Fig. 3f).

3.1.4. Fluorescence quenching of the CQDs

Metal ions are known fluorescence quenchers of CQDs, making them candidates for designing various optical sensors based on visual observation of PL turn-off and/or turn-on. Fluorescence quenching of 17.5 mg/mL pure, 11 mg/mL S-doped and 2.5 mg/mL P-doped CQDs was monitored against CuSo$_4$, CaCl$_2$, ZnCl$_2$, HgCl$_2$, FeCl$_3$, PbCl$_2$, FeSo$_4$ ions solutions respectively (Fig. 4a, b and 4c). As a
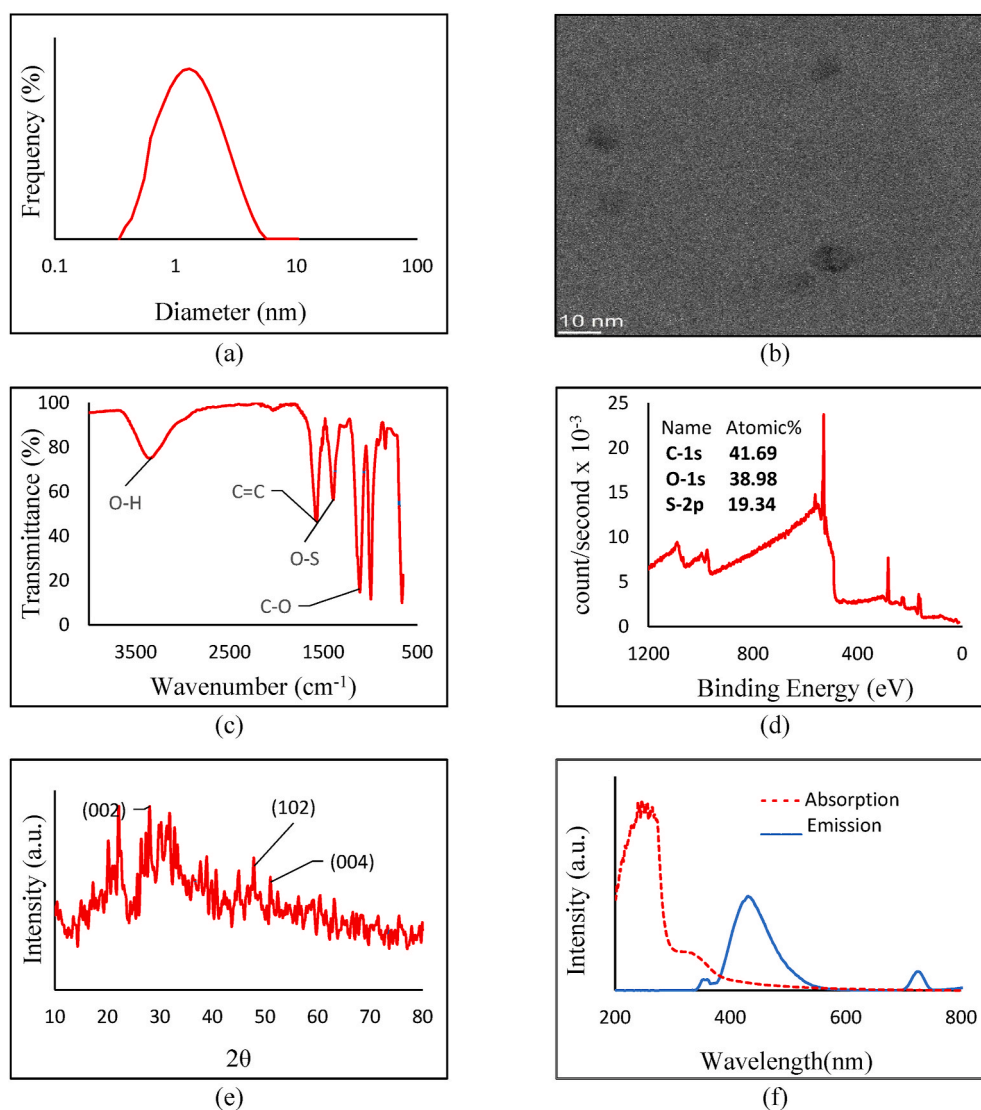
Fig. 2. (a) DLS, (b) TEM, (c) FTIR, (d) XPS, (e) XRD, and (f) PL absorption/emission of S-doped CQD.

result, the fluorescent emission of pure, S-doped and P-doped CQDs were quenched by 6.6 mM Hg^{2+} ions, 12 mM Cu^{2+} ions and 4 mM Fe^{3+} ions, respectively (Fig. 4). The fluorescence quenching mechanism occurs due to the electron, charge or energy transfer resulting from CQD-metal ions interactions. The mechanism of this interaction is based on the fact that the metal ions introduced to the system, selectively interact with the surface hydroxyl and carboxyl functional groups of CQDs. Due to this interaction, the electronic structure of CQDs changes and the distribution of excitons alters, which subsequently leads to a non-radiative charge or energy transfer through the recombination of the electrons and excitons on the surface areas, and quenching of the fluorescence emission [64].

3.2. Study the CQDs and enzyme interaction

In order to study the CQD/enzyme interaction, a CCD-based analysis was performed. So that the D_f % of the 33 designed experiments were calculated (Table 2).

As shown in the data variance analysis table (Table 3), the designed model is valid with a value of 0.0001. Among the individual factors, the time (A) and the type of the CQD (C) are the most effective factors. Among the two-way factors, the simultaneous effect of CQD-type and the CQD/En ratio (BC) are the most influential factors. The value of Lack of Fit, which is an indicator of test error, is insignificant and indicates the absence of any systematic and clear error in this study. In order to understand the synergy and variational influences of the factors on the response, the response surface diagrams based on D_f % were traced for each CQD (Fig. 5).

As can be seen in Fig. 5a, in pure CQD, the response value is obtained in a shorter interaction time and a lower percentage of CQD/En ratio. Meanwhile, the response decreases with the increase of interaction time interval and CQD/En ratio. In Fig. 5b and c, similar
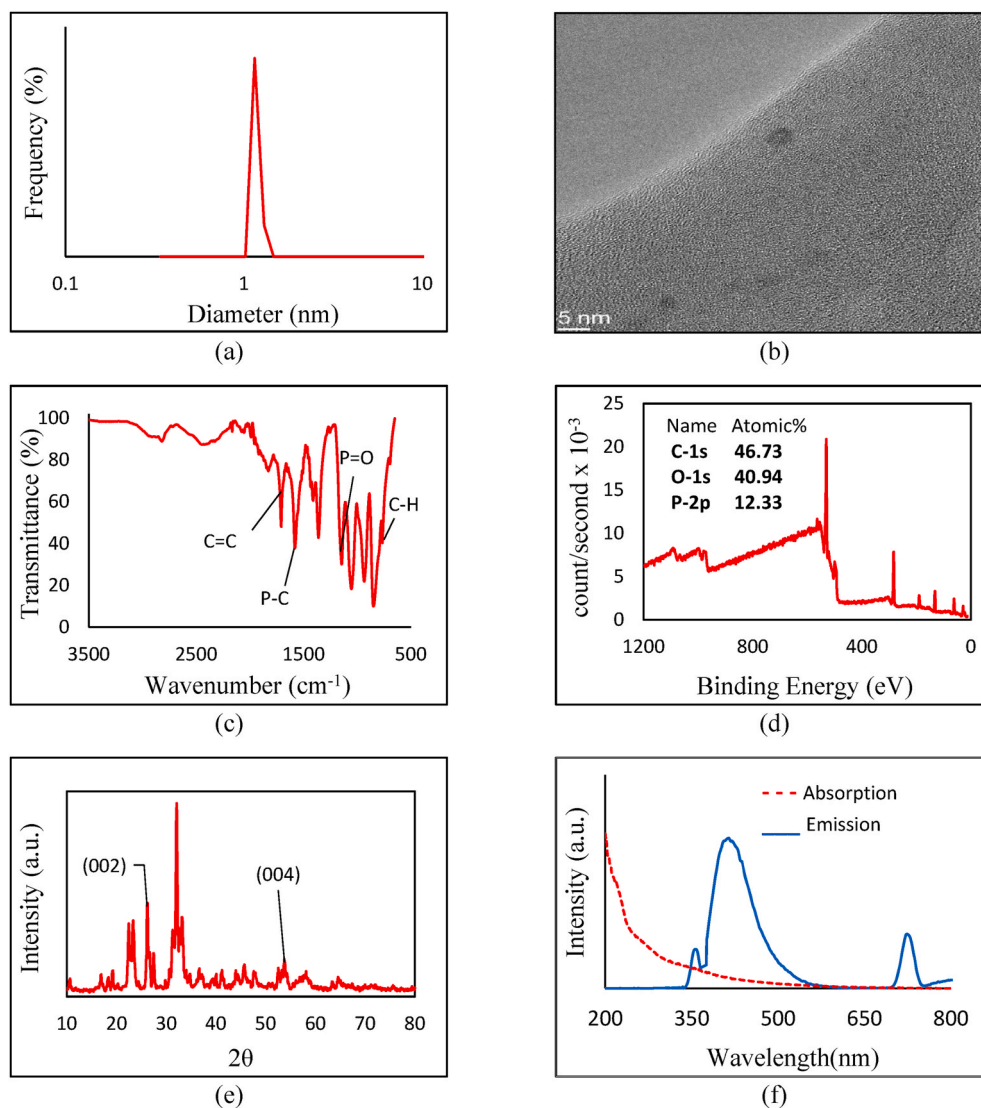
Fig. 3. (a) DLS, (b) TEM, (c) FTIR, (d) XPS, (e) XRD, and (f) PL absorption/emission of P-doped CQD.

behavior can be seen in the case of S-doped and P-doped nanoparticles. In both cases, the greatest response is related to the application of a higher percentage of CQD/En ratio, in a short period of time. In this type, as the duration of the interaction increases, the response drops sharply. Whereas reducing the CQD/En ratio in a short time does not have a significant effect on the response. As can be seen in Fig. 5d and e, with the increase of interaction time and the CQD/En ratio, respectively, the D_f % decreases in all three CQD types. The reduction in D_f % on CQD-pure is much higher than the other types.

3.3. AChE screening based on S-doped CQDs

After examining the D_f % for different CQDs two experiments were suggested by Design Expert software as the most influential conditions. The proposed software experiments include the interaction of S-doped in 4% ratio with enzyme for 3 min and the interaction of enzyme and pure CQD at 16% ratio for 3 min. The results demonstrate that S-doped had the highest emission intensity and was quenched in the shortest time in the presence of Cu^{2+} ions. The proposed experiments were performed as follows: In the first step, the S-doped CQD's PL emission intensity was recorded at 450 nm. Then, Cu^{2+} was added, so that the carboxyl group of S-doped CQDs bound to Cu^{2+} ions, and the emission intensity drops dramatically. After that, ATCh was added to the solution. Finally, by adding AChE, ATCh was hydrolyzed to TCh and acetate, forming a Cu-TCh complex. As a result, Cu^{2+} separates from the carboxyl groups on the surface of the S-doped CQD, ceasing the non-radiative recombination of the electrons and excitons on the surface areas and leading to recovery of the PL emission of the CQD. The strength of copper-thiol complexes, including Cu-TCh complex provides a critical insight into how they might affect Cu chemistry in a CQD based sensors. First, TCh is a mercaptan substance which reacts with Cu^{2+} to

(a)

(b)

(c)
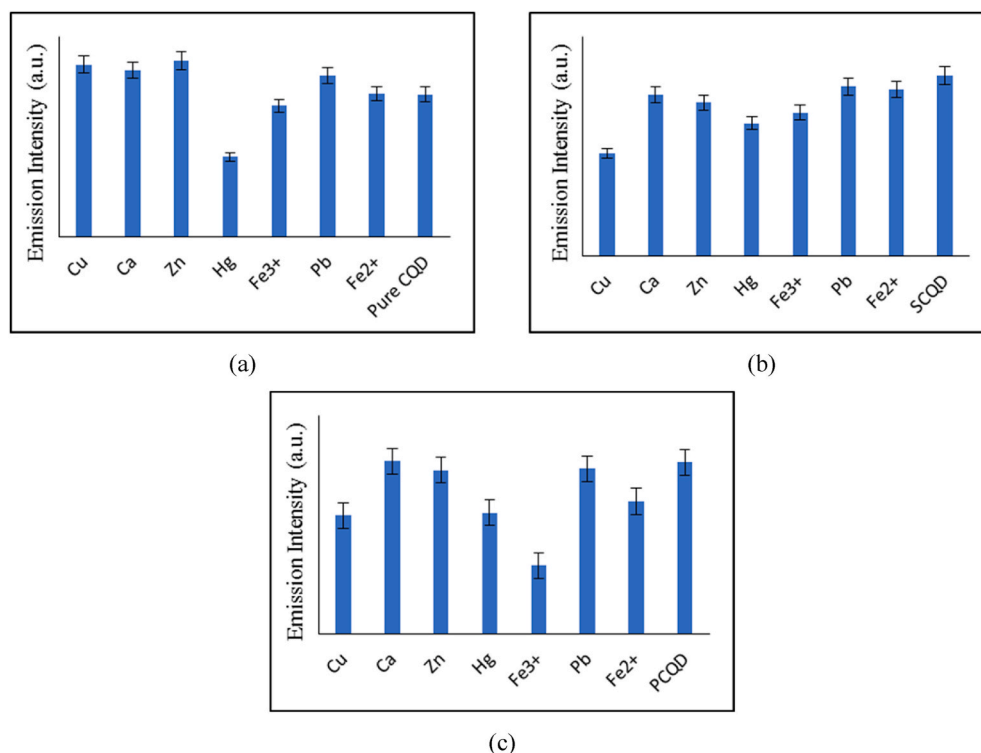
Fig. 4. The change of fluorescent emission of (a) pure, (b) S-doped and (c) P-doped CQDs in the presence of various metal ions.

Table 3
ANOVA for the study of the CQDs interaction Enzyme.

Source	Sum of Squares	df	Mean Square	F Value	p-value Prob > F	
Model	0.031419882	11	0.002856	7.170653	<0.0001	significant
A-Time	0.012526379	1	0.012526	31.44651	<0.0001	
B-CQD/En Ratio	0.003999856	1	0.004	10.04133	0.0046	
C-CQD Type	0.01046129	2	0.005231	13.13113	0.0002	
AB	8.2271E-06	1	8.23E-06	0.020653	0.8871	
AC	0.000682597	2	0.000341	0.856803	0.4388	
BC	0.001222463	2	0.000611	1.534449	0.2388	
ABC	0.00251907	2	0.00126	3.161966	0.0630	
Residual	0.008365125	21	0.000398			
Lack of Fit	0.004616148	15	0.000308	0.492524	0.8754	not significant
Pure Error	0.003748977	6	0.000625			
Cor Total	0.039785007	32				
R-Squared	0.8797		**Adj R-Squared**		0.7969	

form the Cu-TCh complex by the well-known reaction of copper with mercaptans. Furthermore, the strong affinity between thiol and copper can be influenced by the functional groups present in the larger peptide ligands. Walsh and Ahner reported the stability constants for Cu-thiol complexes, using dissociation constant, as the reciprocal of the stability constant. They demonstrated that the addition of a coordinating thiol, increases the affinity value, as reported in Table 4 for some dicysteinal and tripodal cysteine derivatives [65]. In the S-doped CQD/Cu^{2+}/AChE/ATCh system, due to the stronger affinity of Cu^{2+} to form the Cu-TCh complex, PL emission recovery is observed. (Fig. 6a). The increase in the emission intensity after adding ATCh was observed to be time-dependent. However, as shown in Figs. 6b and 10 min was suitable for the catalytic hydrolysis of ATCh by AChE, after which the emission intensity reached a stable state.

3.4. AChE inhibitor screening

For further demonstration of the potential applications of this method, the malathion and chlorpyrifos, known as AChE inhibitors, were selected as samples for proof of concept. The emission intensity of 11 mg/mL S-doped CQD was quenched in the presence of 12
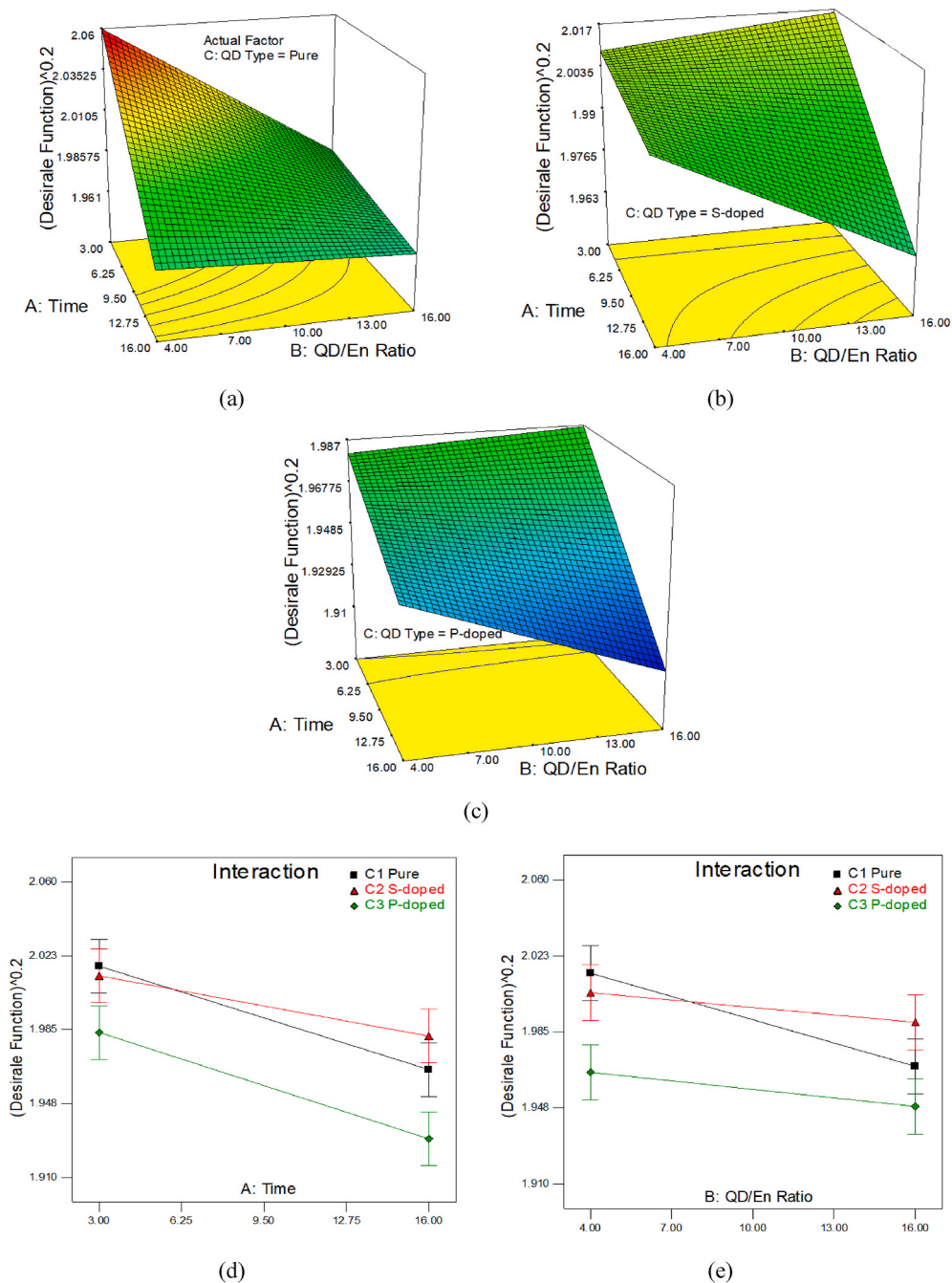
Fig. 5. Comparison of influential factors on D_f, versus A: time and B: CQD/En ratio for C: CQD-types (a) pure, (b) S-doped, and (c) P-doped; and (d) factor AC (time and CQD type); and (e) factor BC (CQD/AChE ratio and CQD type).

mM Cu^{2+} ions. By addition of ATCh and AChE to the system, a significant fluorescence recovery was achieved. However, when 0.005 ppb malathion and 0.002 ppb chlorpyrifos were added to the sensor system, in presence of ATCh and AChE, no apparent fluorescence increase was induced, which clearly demonstrates the inhibitory effect of malathion and chlorpyrifos on AChE. The emission intensity of the sensor system gradually decreases over the increasing inhibitor's concentrations, which further confirms the correlation between AChE inhibition and the concentration of the inhibitors. However, in the presence of AChE inhibitors, ATCh would no longer hydrolyze to TCh and acetate, which in turn leaves Cu^{2+} in interaction with S-doped CQD and the PL emission of the CQD would not be recovered. Therefore, the activity of the AChE and its inhibitor can be well reflected by observing the fluorescence intensity change of S-doped CQD. (Fig. 7a and b).

Table 4
Stability constants for various copper-binding ligands.

Copper binding ligand	Thiol complexation	Technique	Stability constant (K')
GSH	Monothiol	EMF Titration	13.9
Cystein	Monothiol	PGSK Titration	11.1
Arg-Cys	Monothiol	PGSK Titration	11
Gln-Cys	Monothiol	PGSK Titration	11.4
DTT	Dithiol	BCS Titration	15.3
Synthetic dicysteinal peptides	Dithiol	BCS Titration	15.5–16.7
Tripodal-cysteine	Trithiol	BCS Titration	18.8–19.2
GSH_3	Trithiol	BCS Titration	18.8
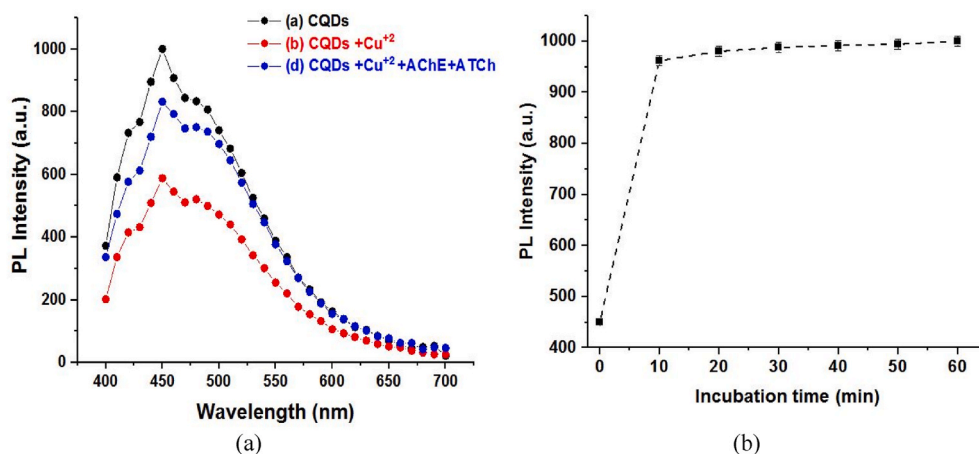
Fig. 6. Variations on PL intensity of CODs (a) in the presence of different compositions, and (b) at various incubation periods.

3.4.1. Proof of concept

Our results indicate that the designated AChE monitoring system can be used to screen the existence of AChE inhibitors, such as malathion and chlorpyrifos, as provided in Fig. 7a and b, respectively, where various concentrations of the mentioned OPs were introduced to the designed sensing system. The calibration plot derived from AChE inhibitor screening plots is presented in Fig. 8. Linear behavior of designed biosensor through various concentrations of inhibitors indicated the reliable performance of developed platform for detection of malathion and chlorpyrifos. The magnitude of LOD using Eq. (2) for malathion and chlorpyrifos were obtained as 1.70 ppb and 1.50 ppb, respectively (Fig. 8a and b). The proposed biosensor achieved a wide linear dynamic range from 5 to 300 ppb in 10 min analysis time, which demonstrates reliable and significant performance.

3.4.2. Selectivity for OPs

Biosensor selectivity was assessed by examining the S-doped CQD/Cu^{2+}/ATCh system in the presence of 50 μL AChE, 0.300 ppb malathion, 0.250 ppb chlorpyrifos, 1.000 ppb alkaline phosphatase, 2.500 ppb NaCl, 0.5 μL DNA, and 0.066 ppb BSA. As shown in Fig. 9, emission intensity increased in the presence of AChE, due to the hydrolysis of ATCh to thiocholine and the binding of Cu^{2+} ions to thiols groups. Moreover, by addition of each mentioned substances, the emission intensity didn't show a significant change. Consequently, the designed biosensor system is specific to detect the AChE inhibitors through the AChE enzyme.

Comparison of the proposed biosensor, based on the S-doped CQD/Cu^{2+}/AChE/ATCh system to previous fluorometric assay biosensors, reported for AChE's inhibitors is presented in Table 5. Compared to previous works, this study developed the biosensor that can provide a significantly lower LOD for quantitative analysis of malathion and chlorpyrifos. Furthermore, the designed sensor offers a shorter processing time, making a fast-response biosensor.

4. Conclusions

In summary, our study has successfully demonstrated a carbon quantum dot-based sensor for the detection of AChE and its inhibitors. The designed sensor took the advantage of the competitive coordination between the affinity of Cu^{2+} ions to the carboxyl groups on the surface of the carbon quantum dots and the thiocholine. The detection strategy was employed for AChE, by emitting a fluorescence signal in combination with its catalytic hydrolysis ability to ATCh. Upon the addition of malathion and chlorpyrifos, the OPs react with AChE to inhibit its activity, resulting in a very poor fluorescence response. This biosensor highlighted a sensitive, specific and rapid detection of malathion and chlorpyrifos, with the LOD of 1.70 ppb and 1.50 ppb, respectively, that was lower than the previously published investigations. Based on our state of knowledge, the organophosphate malathion and chlorpyrifos have not
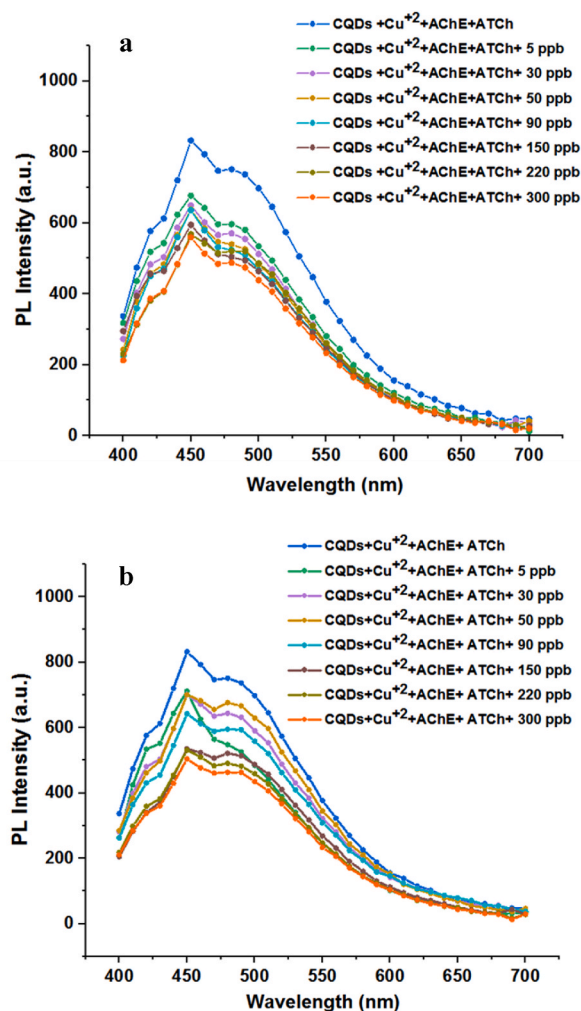
Fig. 7. Change of fluorescence spectra versus various concentrations of (a) malathion and (b) chlorpyrifos.
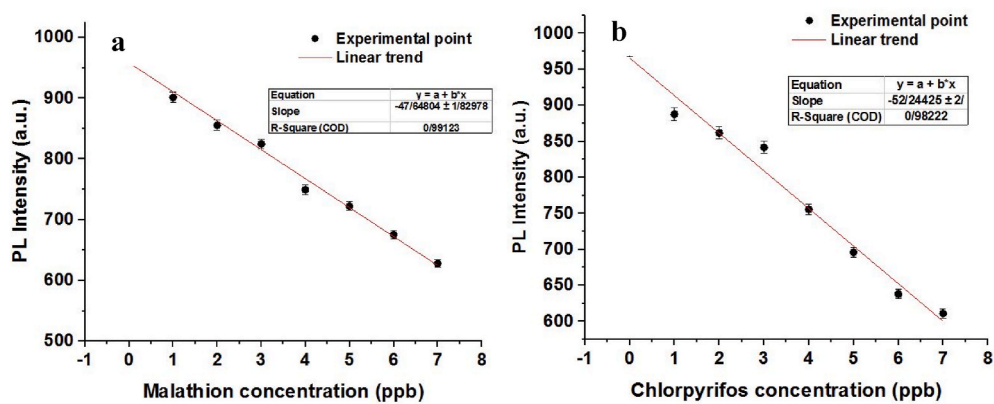
Fig. 8. Calibration plot of CQD designed sensor versus various concentrations of (a) malathion and (b) chlorpyrifos.

been previously reported to be detected with this state of achievement in terms of analysis processing time and LOD, which is crucial in environmental assessments. This study provides a mid-stage platform to develop a convenient, low-cost and ultrasensitive fluorometric device using S-doped CQD/Cu^{2+}/AChE/ATCh system for detection of target OP pesticides residues in agricultural products.
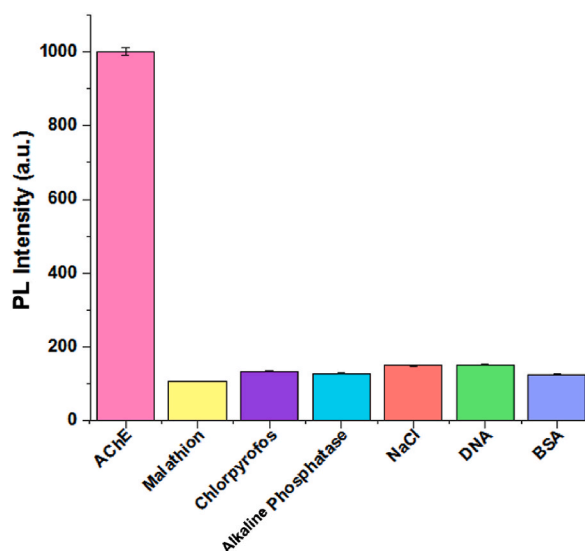
Fig. 9. Emission intensity of S-doped CQD/Cu^{2+}/ATCh system with some interfering substances.

Table 5
Analytical comparison of the performance of the designed sensor.

Main examine reagent	Activity/Detection limit (as reported)	Time	Type of OP	Reference
CQD	1.70 ppb	10 min	Malathion	**This study**
	1.50 ppb		Chlorpyrifos	
CQD	3 ng/mL	15 min	Chlorpyrifos	[66]
CQD	0.21 ng/mL	25 min	Paraoxon	[67]
	0.46 ng/mL		Chlorpyrifos	
CQD	0.21 ± 0.021 µg/L	120 min	Methyl parathion	[68]
	0.44 ± 0.069 µg/L		Chlorpyrifos	
	0.32 ± 0.033 µg/L		Trichlorfon	
CQD	0.05 nM	20 min	Paraoxon	[69]
	0.10 nM		Malathion	
	0.12 nM		Methamidophos	
	0.13 nM		Carbaryl	
CdTe QD	1.62×10^{-15} M	15 min	Paraoxon	[1]
	75.3×10^{-15} M		Dichlorvos	
	0.23×10^{-9} M		Malathion	
	10.6×10^{-12} M		Triazophos	

Author contribution statement

Niloofar Mahmoudi: Performed the experiments; Analyzed and interpreted the data; Wrote the paper.

Fataneh Fatemi, Moones Rahmandost: Conceived and designed the experiments; Analyzed and interpreted the data; Contributed reagents, materials; analysis tools or data; Wrote the paper.

Fateme Mirzajani: Conceived and designed the experiments; Analyzed and interpreted the data; Wrote the paper.

Seyed Omid Ranaei Siadat: Contributed reagents, materials, analysis tools or data; Wrote the paper.

Data availability statement

Data associated with this study has been deposited at Social Science Research Network (SSRN)https://ssrn.com/abstract%20=%204401576 https://doi.org/10.2139/ssrn.4401576.

Additional information

No additional information is available for this paper.

Ethical approval

This article does not contain any studies with human or animal subjects.

Declaration of competing interest

The authors declare that they have no known competing financial interests or personal relationships that could have appeared to influence the work reported in this paper.

Acknowledgements

References

[1] J. Korram, L. Dewangan, I. Karbhal, R. Nagwanshi, S.K. Vaishanav, K.K. Ghosh, M.L. Satnami, CdTe QD-based inhibition and reactivation assay of acetylcholinesterase for the detection of organophosphorus pesticides, RSC Adv. 10 (2020) 24190–24202, https://doi.org/10.1039/d0ra03055d.

[2] X. Xu, Y. Cen, G. Xu, F. Wei, M. Shi, Q. Hu, A ratiometric fluorescence probe based on carbon dots for discriminative and highly sensitive detection of acetylcholinesterase and butyrylcholinesterase in human whole blood, Biosens. Bioelectron. 131 (2019) 232–236, https://doi.org/10.1016/j.bios.2019.02.031.

[3] J.H. Xuereb, E.K. Perry, J.M. Candy, J.R. Bonham, R.H. Perry, E. Marshall, Parameters of cholinergic neurotransmission in the thalamus in Parkinson's disease and Alzheimer's disease, J. Neurol. Sci. 99 (1990) 185–197, https://doi.org/10.1016/0022-510X(90)90155-G.

[4] M.B. Colovic, D.Z. Krstic, T.D. Lazarevic-Pasti, A.M. Bondzic, V.M. Vasic, Acetylcholinesterase inhibitors: pharmacology and toxicology, Curr. Neuropharmacol. 11 (2013) 315–335.

[5] J. Massoulié, L. Pezzementi, S. Bon, E. Krejci, F.M. Vallette, Molecular and cellular biology of cholinesterases, Prog. Neurobiol. 41 (1993) 31–91, https://doi.org/10.1016/0301-0082(93)90040-Y.

[6] G.B. Koelle, The histochemical localization of cholinesterases in the central nervous system of the rat, J. Comp. Neurol. 100 (1954) 211–235, https://doi.org/10.1002/cne.901000108.

[7] M.Q. Daniel, Acetylcholinesterase: enzyme structure, reaction dynamics, and virtual transition states, Chem. Rev. 87 (1987) 955–979.

[8] Palmer Taylor, Zoran Radii, The CHOLINESTERASES: from genes to proteins, J. Biol. Chem. 266 (1991) 4025–4028, https://doi.org/10.1016/s0021-9258(20)64277-6.

[9] G. Mercey, T. Verdelet, J. Renou, M. Kliachyna, R. Baati, F. Nachon, L. Jean, P.Y. Renard, Reactivators of acetylcholinesterase inhibited by organophosphorus nerve agents, Acc. Chem. Res. 45 (2012) 756–766, https://doi.org/10.1021/ar2002864.

[10] A. Vinotha Alex, A. Mukherjee, Review of recent developments (2018–2020) on acetylcholinesterase inhibition based biosensors for organophosphorus pesticides detection, Microchem. J. 161 (2021), 105779, https://doi.org/10.1016/j.microc.2020.105779.

[11] H. Dvir, I. Silman, M. Harel, T.L. Rosenberry, J.L. Sussman, Acetylcholinesterase: from 3D structure to function, Chem. Biol. Interact. 187 (2010) 10–22, https://doi.org/10.1016/j.cbi.2010.01.042.

[12] Z. Suo, X. Liu, X. Hou, Y. Liu, J. Lu, F. Xing, Y. Chen, L. Feng, Ratiometric assays for acetylcholinesterase activity and organo-phosphorous pesticide based on superior carbon quantum dots and BLGF-protected gold nanoclusters FRET process, ChemistrySelect 5 (2020) 9254–9260, https://doi.org/10.1002/slct.202002042.

[13] A.M. Badr, Organophosphate toxicity: updates of malathion potential toxic effects in mammals and potential treatments, Environ. Sci. Pollut. Res. 27 (2020) 26036–26057, https://doi.org/10.1007/s11356-020-08937-4.

[14] X. Dan, L. Ruiyi, W. Qinsheng, Y. Yongqiang, Z. Haiyan, L. Zaijun, A NiAg-graphene quantum dot-graphene hybrid with high oxidase-like catalytic activity for sensitive colorimetric detection of malathion, New J. Chem. 45 (2021) 7129–7137, https://doi.org/10.1039/d1nj00621e.

[15] F.K. Coban, S. Ince, I. Kucukkurt, H.H. Demirel, O. Hazman, Boron attenuates malathion-induced oxidative stress and acetylcholinesterase inhibition in rats, Drug Chem. Toxicol. 38 (2015) 391–399, https://doi.org/10.3109/01480545.2014.974109.

[16] N. Suresh Babu, J.K. Malik, G.S. Rao, M. Aggarwal, V. Ranganathan, Effects of subchronic malathion exposure on the pharmacokinetic disposition of pefloxacin, Environ. Toxicol. Pharmacol. 22 (2006) 167–171, https://doi.org/10.1016/j.etap.2006.03.001.

[17] J.B. Ortiz-Delgado, V. Funes, C. Sarasquete, The organophosphate pesticide -OP- malathion inducing thyroidal disruptions and failures in the metamorphosis of the Senegalese sole, Solea senegalensis, BMC Vet. Res. 15 (2019) 1–21, https://doi.org/10.1186/s12917-019-1786-z.

[18] T.H. DeLuca, S. Gao, Use of biochar in organic farming, Org. Farming. (2019) 25–49, https://doi.org/10.1007/978-3-030-04657-6_3.

[19] D. Capoferri, F. Della Pelle, M. Del Carlo, D. Compagnone, Affinity sensing strategies for the detection of pesticides in food, Foods (2018) 7, https://doi.org/10.3390/foods7090148.

[20] P.T. Kim Hong, C.H. Jang, Sensitive and label-free liquid crystal-based optical sensor for the detection of malathion, Anal. Biochem. 593 (2020), 113589, https://doi.org/10.1016/j.ab.2020.113589.

[21] S.O. Igbedioh, Effects of agricultural pesticides on humans, animals, and higher plants in developing countries, Arch. Environ. Health 46 (1991) 218–224, https://doi.org/10.1080/00039896.1991.9937452.

[22] O. Abdel-Salam, A. Sleem, E. Youness, F. Morsy, Preventive effects of cannabis on neurotoxic and hepatotoxic activities of malathion in rat, Asian Pac. J. Trop. Med. 11 (2018) 272–279, https://doi.org/10.4103/1995-7645.231467.

[23] S. Kumar, J.G. Sharma, Effect of malathion on seed germination and photosynthetic pigments in wheat (Triticum aestivum L.), Asian J. Appl. Sci. Technol. 1 (2017) 158–167.

[24] S.A.J. Ki-Hyun Kim, Ehsanul Kabir, Exposure to Pesticides and the Associated Human Health Effects, 2017.

[25] P.B. Tchounwou, A.K. Patlolla, C.G. Yedjou, P.D. Moore, Environmental exposure and Health effects associated with malathion toxicity, Toxic. Hazard Agrochem (2015), https://doi.org/10.5772/60911.

[26] The Structural and Biochemical Impact of Monomerizing Human Acetylcholinesterase, (n.d.).

[27] H. Wu, R. Zhang, J. Liu, Y. Guo, E. Ma, Effects of malathion and chlorpyrifos on acetylcholinesterase and antioxidant defense system in Oxya chinensis (Thunberg) (Orthoptera: acrididae), Chemosphere 83 (2011) 599–604, https://doi.org/10.1016/j.chemosphere.2010.12.004.

[28] M.I. Gaviria, K. Barrientos, J.P. Arango, J.B. Cano, G.A. Peñuela, Highly sensitive fluorescent biosensor based on acetylcholinesterase and carbon dots–graphene oxide quenching test for analytical and commercial organophosphate pesticide detection, Front. Environ. Sci. 10 (2022), https://doi.org/10.3389/fenvs.2022.825112.

[29] H. Ubaid ur Rahman, W. Asghar, W. Nazir, M.A. Sandhu, A. Ahmed, N. Khalid, A comprehensive review on chlorpyrifos toxicity with special reference to endocrine disruption: evidence of mechanisms, exposures and mitigation strategies, Sci. Total Environ. 755 (2021), 142649, https://doi.org/10.1016/j.scitotenv.2020.142649.

[30] A. Şişecioğlu, M. Şişecioğlu, M. Atamanalp, A. Işik, B. Yilmaz, The in vitro and in vivo effects of chlorpyrifos on acetylcholinesterase activity of rainbow trout brain, J. Appl. Anim. Res. 44 (2016) 243–247, https://doi.org/10.1080/09712119.2015.1031776.

[31] T.C. Kwong, Organophosphate pesticides: biochemistry and clinical toxicology, Ther. Drug Monit. 24 (2002) 144–149, https://doi.org/10.1097/00007691-200202000-00022.

[32] Y. Miao, N. He, J.J. Zhu, History and new developments of assays for cholinesterase activity and inhibition, Chem. Rev. 110 (2010) 5216–5234, https://doi.org/10.1021/cr900214c.

[33] G.L. Ellman, K.D. Courtney, V. Andres, R.M. Featherstone, A new and rapid colorimetric determination of acetylcholinesterase activity, Biochem. Pharmacol. 7 (1961) 88–95, https://doi.org/10.1016/0006-2952(61)90145-9.

[34] H. Li, Y. Guo, L. Xiao, B. Chen, A fluorometric biosensor based on H2O2-sensitive nanoclusters for the detection of acetylcholine, Biosens. Bioelectron. 59 (2014) 289–292, https://doi.org/10.1016/j.bios.2014.03.054.

[35] S. Hou, Z. Ou, Q. Chen, B. Wu, Amperometric acetylcholine biosensor based on self-assembly of gold nanoparticles and acetylcholinesterase on the sol-gel/multi-walled carbon nanotubes/choline oxidase composite-modified platinum electrode, Biosens. Bioelectron. 33 (2012) 44–49, https://doi.org/10.1016/j.bios.2011.12.014.

[36] Z. Chen, X. Ren, X. Meng, L. Tan, D. Chen, F. Tang, Quantum dots-based fluorescent probes for turn-on and turn-off sensing of butyrylcholinesterase, Biosens. Bioelectron. 44 (2013) 204–209, https://doi.org/10.1016/j.bios.2013.01.034.

[37] Z. Qian, L. Chai, C. Tang, Y. Huang, J. Chen, H. Feng, A fluorometric assay for acetylcholinesterase activity and inhibitor screening with carbon quantum dots, Sensors Actuators, B Chem. 222 (2016) 879–886, https://doi.org/10.1016/j.snb.2015.09.023.

[38] D. Liao, J. Chen, H. Zhou, Y. Wang, Y. Li, C. Yu, In situ formation of metal coordination polymer: a strategy for fluorescence turn-on assay of acetylcholinesterase activity and inhibitor screening, Anal. Chem. 85 (2013) 2667–2672, https://doi.org/10.1021/ac302971x.

[39] L. Peng, G. Zhang, D. Zhang, J. Xiang, R. Zhao, Y. Wang, D. Zhu, A fluorescence "turn-on" ensemble for acetylcholinesterase activity assay and inhibitor screening, Org. Lett. 11 (2009) 4014–4017, https://doi.org/10.1021/ol9016723.

[40] S. Sabelle, P.Y. Renard, K. Pecorella, S. De Suzzoni-Dézard, C. Créminon, J. Grassi, C. Mioskowski, Design and synthesis of chemiluminescent probes for the detection of cholinesterase activity, J. Am. Chem. Soc. 124 (2002) 4874–4880, https://doi.org/10.1021/ja0171299.

[41] M. Wang, X. Gu, G. Zhang, D. Zhang, D. Zhu, Convenient and continuous fluorometric assay method for acetylcholinesterase and inhibitor screening based on the aggregation-induced emission, Anal. Chem. 81 (2009) 4444–4449, https://doi.org/10.1021/ac9002722.

[42] Y. Zhang, Y. Cai, Z. Qi, L. Lu, Y. Qian, DNA-templated silver nanoclusters for fluorescence turn-on assay of acetylcholinesterase activity, Anal. Chem. 85 (2013) 8455–8461, https://doi.org/10.1021/ac401966d.

[43] D.Z.M. Wang, X. Gu, G. Zhang, D. Zhang, Continuous colorimetric assay for acetylcholinesterase and inhibitor screening with gold nanoparticles, Langmuir (2009) 2504–2507, https://doi.org/10.1039/c1an15224f.

[44] D. Liu, W. Chen, Y. Tian, S. He, W. Zheng, J. Sun, Z. Wang, X. Jiang, A highly sensitive gold-nanoparticle-based assay for acetylcholinesterase in cerebrospinal fluid of transgenic mice with alzheimer's disease, Adv. Healthc. Mater. 1 (2012) 90–95, https://doi.org/10.1002/adhm.201100002.

[45] W. Li, W. Li, Y. Hu, Y. Xia, Q. Shen, Z. Nie, Y. Huang, S. Yao, A fluorometric assay for acetylcholinesterase activity and inhibitor detection based on DNA-templated copper/silver nanoclusters, Biosens. Bioelectron. 47 (2013) 345–349, https://doi.org/10.1016/j.bios.2013.03.038.

[46] H. Li, Y. Guo, L. Xiao, B. Chen, Selective and sensitive detection of acetylcholinesterase activity using denatured protein-protected gold nanoclusters as a label-free probe, Analyst 139 (2014) 285–289, https://doi.org/10.1039/c3an01736b.

[47] R. Gill, L. Bahshi, R. Freeman, I. Willner, Optical detection of glucose and acetylcholine esterase inhibitors by H2O2-sensitive CdSe/ZnS quantum dots, Angew. Chemie - Int. Ed. 47 (2008) 1676–1679, https://doi.org/10.1002/ange.200704794.

[48] L. Saa, A. Virel, J. Sanchez-Lopez, V. Pavlov, Analytical applications of enzymatic growth of quantum dots, Chem. Eur J. 16 (2010) 6187–6192, https://doi.org/10.1002/chem.200903373.

[49] F. Feng, Y. Tang, S. Wang, Y. Li, D. Zhu, Continuous fluorometric assays for acetylcholinesterase activity and inhibition with conjugated polyelectrolytes, Angew. Chemie - Int. Ed. 46 (2007) 7882–7886, https://doi.org/10.1002/anie.200701724.

[50] C. Lei, Z. Wang, Z. Nie, H. Deng, H. Hu, Y. Huang, S. Yao, Resurfaced fluorescent protein as a sensing platform for label-free detection of copper(II) ion and acetylcholinesterase activity, Anal. Chem. 87 (2015) 1974–1980, https://doi.org/10.1021/ac504390e.

[51] W. Zhang, L. Zhu, J. Qin, C. Yang, Novel water-soluble red-emitting poly(p-phenylenevinylene) derivative: synthesis, characterization, and fluorescent acetylcholinesterase assays, J. Phys. Chem. B 115 (2011) 12059–12064, https://doi.org/10.1021/jp206930v.

[52] J. Shen, Y. Zhu, X. Yang, C. Li, Graphene quantum dots: emergent nanolights for bioimaging, sensors, catalysis and photovoltaic devices, Chem. Commun. 48 (2012) 3686–3699, https://doi.org/10.1039/c2cc00110a.

[53] Z. Qian, L. Chai, C. Tang, Y. Huang, J. Chen, H. Feng, Carbon quantum dots-based recyclable real-time fluorescence assay for alkaline phosphatase with adenosine triphosphate as substrate, Anal. Chem. 87 (2015) 2966–2973, https://doi.org/10.1021/ac504519b.

[54] S.N. Baker, G.A. Baker, Luminescent carbon nanodots: emergent nanolights, Angew. Chemie - Int. Ed. 49 (2010) 6726–6744, https://doi.org/10.1002/anie.200906623.

[55] V.C. Hoang, K. Dave, V.G. Gomes, Carbon quantum dot-based composites for energy storage and electrocatalysis: mechanism, applications and future prospects, Nano Energy 66 (2019), 104093, https://doi.org/10.1016/j.nanoen.2019.104093.

[56] S.Y. Lim, W. Shen, Z. Gao, Carbon quantum dots and their applications, Chem. Soc. Rev. 44 (2015) 362–381, https://doi.org/10.1039/c4cs00269e.

[57] A. Zhao, Z. Chen, X. Qu, C. Zhao, N. Gao, Recent advances in bioapplications of C-dots, Carbon N. Y. 85 (2014) 309–327, https://doi.org/10.1016/j.carbon.2014.12.045.

[58] X.T. Zheng, A. Ananthanarayanan, K.Q. Luo, P. Chen, Glowing graphene quantum dots and carbon dots: properties, syntheses, and biological applications, Small 11 (2015) 1620–1636, https://doi.org/10.1002/smll.201402648.

[59] Y. Wang, L. Zhang, R.P. Liang, J.M. Bai, J.D. Qiu, Using graphene quantum dots as novel photoluminescent probes for protein kinase sensing, Anal. Chem. 85 (2013) 9148–9155, https://doi.org/10.1021/ac401807b.

[60] S. Liu, N. Zhao, Z. Cheng, H. Liu, Amino-functionalized green fluorescent carbon dots as surface energy transfer biosensors for hyaluronidase, Nanoscale 7 (2015) 6836–6842, https://doi.org/10.1039/c5nr00070j.

[61] Z.S. Qian, L.J. Chai, Y.Y. Huang, C. Tang, J. Jia Shen, J.R. Chen, H. Feng, A real-time fluorescent assay for the detection of alkaline phosphatase activity based on carbon quantum dots, Biosens. Bioelectron. 68 (2015) 675–680, https://doi.org/10.1016/j.bios.2015.01.068.

[62] Q. Xu, P. Pu, J. Zhao, C. Do, Preparation of highly photoluminescent sulfur-doped carbon dots for Fe(III) detection, Mater. Chem. A. 3 (2014) 542–546, https://doi.org/10.1039/C4TA05483K.

[63] D. Shi, F. Yan, Y. Wang, X. Zhou, L. Chen, P-doped carbon dots act as nanosensor for trace 2,4,6-trinitrophenol detection and fluorescent reagent for biological imaging, RSC Adv. 5 (2015) 98492–98499, https://doi.org/10.1039/C5RA18800H.

[64] N. Liang, X. Hu, W. Li, A.W. Mwakosya, Z. Guo, Y. Xu, X. Huang, Z. Li, X. Zhang, X. Zou, J. Shi, Fluorescence and colorimetric dual-mode sensor for visual detection of malathion in cabbage based on carbon quantum dots and gold nanoparticles, Food Chem. 343 (2021), 128494, https://doi.org/10.1016/j.foodchem.2020.128494.

[65] Michael J. Walsh, Beth A. Ahner, Determination of stability constants of Cu(I), Cd(II) & Zn(II) complexes with thiols using fluorescent probes, J. Inorg. Biochem. 128 (2013) 112–123, https://doi.org/10.1016/j.jinorgbio.2013.07.012.

[66] B. Lin, Y. Yan, M. Guo, Y. Cao, Y. Yu, T. Zhang, Y. Huang, D. Wu, Modification-free carbon dots as turn-on fluorescence probe for detection of organophosphorus pesticides, Food Chem. 245 (2018) 1176–1182, https://doi.org/10.1016/j.foodchem.2017.11.038.

[67] B. Reshma, R. Gupta, K.K. Sharma, Ghosh, Facile and visual detection of acetylcholinesterase inhibitors by carbon quantum dots, New J. Chem. 43 (2019) 9924–9933, https://doi.org/10.1039/C9NJ02347J.

[68] M. Jiang, J. He, J. Gong, H. Gao, Z. Xu, Development of a quantum dot-labelled biomimetic fluorescence immunoassay for the simultaneous determination of three organophosphorus pesticide residues in agricultural products, Food Agric. Immunol. 30 (2019) 248–261, https://doi.org/10.1080/09540105.2019.1572714.

[69] K.K.G. Jyoti Korrama, Lakshita Dewangana, Rekha Nagwanshib, Indrapal Karbhala, M.L. Satnamia*, rCarbon Quantum Dot-Gold Nanoparticle System as Probe for Inhibition and Reactivation of Acetylcholinesterase: Detection of Pesticides, 2019, https://doi.org/10.1039/C9NJ00555B.